# A 200 GHz Fully Integrated, Polarization-Resolved Quasi-Optical Detector Using Zero-Bias Heterostructure Backward Diodes

Yu Shi<sup>®</sup>, Yijing Deng, Peizhao Li<sup>®</sup>, Graduate Student Member, IEEE, Patrick Fay<sup>®</sup>, Fellow, IEEE, and Lei Liu<sup>®</sup>, Senior Member, IEEE

Abstract—We report the design, fabrication, and prototype demonstration of a 200-GHz polarization-resolved quasioptical detector employing monolithically integrated zero-bias heterostructure backward diodes (HBDs). In this design, polarization resolution is achieved by orthogonally integrating the detectors with a planar dual-polarization annular-slot antenna. The detector chip was fabricated and mounted on an extended hemispherical Si lens to enhance antenna efficiency in the millimeter-wave to terahertz region. The responsivity and radiation patterns of the detector were characterized experimentally; good agreement with theoretical calculations was obtained. By measuring the outputs of two orthogonal HBDs as a function of the polarization angle of the incident wave, the planar detector detects intensity and resolves polarization. On the basis of the polarimetric measurement, we further demonstrate the polarization imaging capability of the proposed detector by using it as an imaging system. The detector is promising for developing terahertz polarimetric sensors and imaging arrays in chemical sensing, biomedical imaging, and radio astronomy applications.

Index Terms—Backward diodes, polarization-resolved detector, quasi-optical technology, terahertz sensing and imaging.

## I. Introduction

ILLIMETER-WAVE to terahertz (mmW-THz) detectors are needed for a variety of fields including radio astronomy, biological sensing, medical imaging, and security surveillance [1]-[4]. However, most detectors demonstrated to date sense only the amplitude and/or phase of the incident electromagnetic (EM) waves, without obtaining polarization information. The polarization shift due to birefringence, oblique incidence, and multiple scattering can provide useful information about the object under test [5], which leads to an increasing interest in high-performance, polarization sensitive detectors. Superconductor-insulator-superconductor mixers with an orthomode transducer [6], feedhorn-coupled, orthogonally spaced microwave kinetic inductance detectors [7], and SiGe HBT detectors with dual polarization on-chip antennas [8], [9] have been employed for potential polarization detection in the mmW-THz region. However, the first two designs require bulky horn antennas and must operate

Manuscript received January 12, 2022; accepted February 22, 2022. Date of publication March 16, 2022; date of current version July 7, 2022. This work was supported in part by the National Science Foundation under Grant ECCS-1508057, Grant ECCS-1711631, and Grant ECCS-1711052. (Corresponding author: Yu Shi.)

The authors are with the Electrical Engineering Department, University of Notre Dame, Notre Dame, IN 46556 USA (e-mail: yshi5@nd.edu).

Color versions of one or more figures in this letter are available at https://doi.org/10.1109/LMWC.2022.3155959.

Digital Object Identifier 10.1109/LMWC.2022.3155959

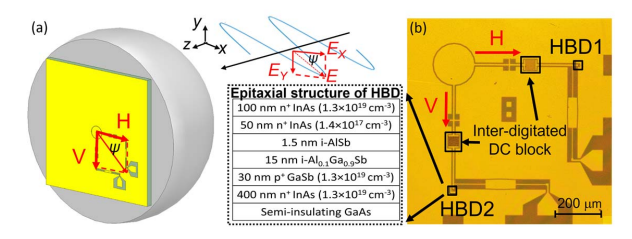


Fig. 1. (a) Schematic of the polarization-resolved detector. (b) Layout of the detector using two orthogonal feeds of HBDs, matching networks, and interdigitated dc blocks. Inset: schematic of HBD epitaxial structure.

in cryogenic conditions, whereas HBT needs additional biasing circuits that increase the 1/f noise as well as the complexity and power consumption of the imaging system. In addition, polarization imaging, which was generally performed by using THz time-domain spectroscopy (TDS) systems [10], [11], has not yet been demonstrated by using incoherent detectors.

To circumvent the limitations of existing devices, we demonstrate a fully integrated and polarization-resolved detector using two channels (one for horizontal polarization, H, and one for vertical, V) based on zero-bias heterostructure backward diodes (HBDs) and a planar dual-polarization annular-slot antenna (ASA). The concept and die photo are shown in Fig. 1. The HBDs (see epitaxial structure in Fig. 1 inset) offer the potential for superior detection performance (e.g., record-high zero-bias curvature coefficient  $(\gamma)$  [12] for high responsivity and low noise equivalent power (NEP, 0.18 pW/Hz $^{1/2}$  [13]), with cutoff frequency as high as 8 THz [14]), leading to highly sensitive, real-time, and room temperature mmW-THz detection [15]. The use of two orthogonal channels further enables the polarization of the incident EM wave to be resolved by simultaneously measuring the two orthogonally polarized components. Additionally, the proposed detector can be easily expanded to develop a focal-plane array (FPA) owing to its compact size and planar structure.

In this letter, the design, fabrication, and characterization of a prototype 200-GHz detector are presented. Although the responsivity in experiment has not yet been optimized, as a prototype demonstration we successfully show that such a detector with ASA and interdigitated dc block can not only measure the incident power but also resolve the polarization of the incoming waves. We further demonstrate the polarization imaging capability of the proposed detector by scanning the transmitting field of a rotated horn antenna as an imaging system. The integrated planar detector presented here is promising to develop polarimetric sensors and advanced

1531-1309 © 2022 IEEE. Personal use is permitted, but republication/redistribution requires IEEE permission. See https://www.ieee.org/publications/rights/index.html for more information.

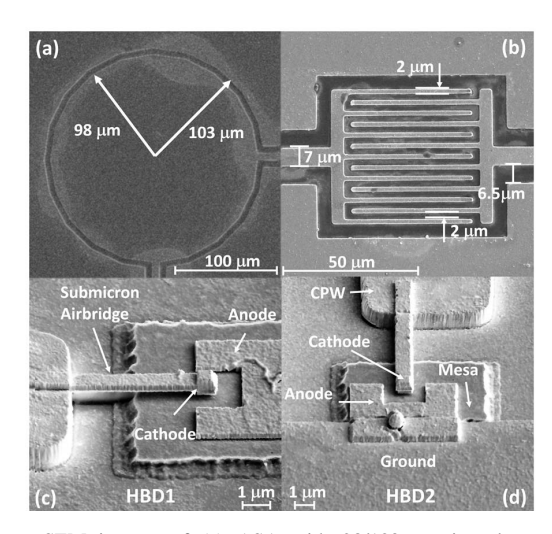


Fig. 2. SEM images of (a) ASA with 98/103- $\mu$ m inner/outer radius, (b) interdigitated dc block with 2- $\mu$ m finger/gap, and 0.8  $\mu$ m × 0.8  $\mu$ m HBD with submicrometer-scale airbridge, a three-sided wraparound anode contact, and 6  $\mu$ m × 8  $\mu$ m mesa in the (c) horizontal (H) and (d) vertical (V) channel HBDs.

FPAs for chemical sensing, biomedical imaging, and radio astronomy in the mmW-THz region.

## II. DETECTOR DESIGN

For the detector design to resolve incident wave polarization, a two-channel detector circuit that includes shorted-stub impedance matching networks, interdigitated dc blocks, HBDs, and three-stage low-pass filters was designed and integrated with a dual polarization ASA, as shown in Fig. 1(b).

The planar ASA [a detailed view of which is shown in Fig. 2(a)] has been experimentally demonstrated for dual-polarization operation, with port-to-port isolation of 25 dB [16]. For operation of the prototype at 200 GHz, the inner and outer radii of the ASA were designed to be 98 and 103  $\mu$ m, respectively, leading to a slot size of 5  $\mu$ m. To couple the RF power out of the antenna, two orthogonally oriented 50  $\Omega$  (at 200 GHz) coplanar waveguide (CPW) transmission lines feeds with a center conductor width of 7  $\mu$ m and a gap width of 6.5  $\mu$ m were used. A single stub impedance matching network, including a 2-μm finger/gap interdigitated capacitor as the dc block [Fig. 2(b)], was designed to match the impedance of the antenna ( $\sim$ 100  $\Omega$ ) to that of HBD ( $\sim$ 124 -i330  $\Omega$  from the device model in [13]). A three-stage stepped-impedance low-pass video filter was also included to filter out the 200-GHz carrier from the baseband output. In this design, the two channels are RF isolated to detect two orthogonal linear polarization components independently, while the dc signals are separated by the interdigitated dc blocks, instead of a split capacitor on the antenna [16]. The detector occupies a total area of 900  $\mu$ m × 900  $\mu$ m and features only planar circuitry for potential expansion into 2-D imaging arrays.

The fully integrated HBDs employed here utilize the broken-gap energy band alignment between InAs and Al<sub>0.1</sub>Ga<sub>0.9</sub>Sb (see Fig. 1 inset) to create a highly nonlinear tunneling current around zero bias, resulting in high curvature coefficient [13]. Low-series resistance can be achieved with the tunneling contact between InAs and GaSb. In addition, submicrometer-scale airbridges and a optimized device layout [see the SEM images in Fig. 2(c) and (d)] were employed to reduce the parasitic capacitance and spreading resistance

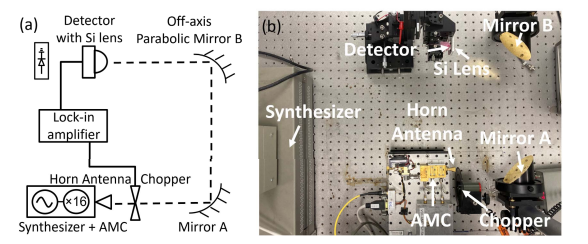


Fig. 3. (a) Schematic and (b) actual measurement setup for RF testing.

and improve the achievable detector responsivity and cutoff frequency [12], [14].

#### III. DETECTOR FABRICATION AND INTEGRATION

The designed detector was fabricated based on the process described in [12]. In short, the two  $0.8~\mu m \times 0.8~\mu m$  active area HBDs were defined with electron-beam lithography, followed by cathode contact deposition. A self-aligned wet etch process was used to fabricate the diode junction. The wraparound anodes, as well as the ASA and passive elements, were then deposited. The submicrometer-scale airbridges were fabricated by liftoff after benzocyclobutene (BCB) passivation and released when the BCB sacrificial layer was removed through dry etch. Finally, the detector was mounted onto an extended hemispherical Si lens with a radius of 5 mm (extension length of 1.5 mm) for high-efficiency Gaussian coupling in the mmW-THz region [16].

# IV. DETECTOR TESTING AND CHARACTERIZATION A. DC Testing

In order to characterize the nonlinearity of the HBDs, the dc on wafer measurement was first carried out by using the probe station with an HP4155 semiconductor parameter analyzer. A zero-bias curvature coefficient ( $\gamma$ ) of  $-10~V^{-1}$  was achieved for HBD1 in H channel, whereas that for HBD2 was  $-7~V^{-1}$ .

# B. RF Testing

The schematic and the experiment setup for characterizing the RF performance of the detector are shown in Fig. 3(a) and (b), respectively. The THz beam (190–210 GHz) was generated by an HP83712B synthesized generator with a VDI (Virginia Diodes, Inc.) multiplier chain (VDI-AMC-S215b) and transmitted through a WR-5.1 horn antenna. A chopper was placed at the output of the transmitter horn to modulate the RF power. The beam was then collimated by an off-axis parabolic mirror (mirror A in Fig. 3(b) and the focal length is 8.8 cm) and coupled onto the integrated detector through a second mirror with the same parameters (mirror B). The dc output of the detector was measured by a lock-in amplifier, as shown in Fig. 3(a).

In the experiment, the H-polarization channel of the detector was first aligned with the E-plane of the transmitting horn antenna [see Fig. 3(b)] for maximum responsivity, whereas that of V-polarization was minimum. Then, the detector was rotated 90° along the polar axis of the Si lens, so that the V channel reached its peak. The measured responsivity versus frequency for each channel is plotted in Fig. 4(a). The detector was also simulated in Keysight Advanced Design System (ADS) software. In this simulation, HBDs are represented as the lumped element model [13] with bias-dependent junction resistance obtained from dc testing. The ASA is treated as the RF source using the simulated antenna radiation spectrum as

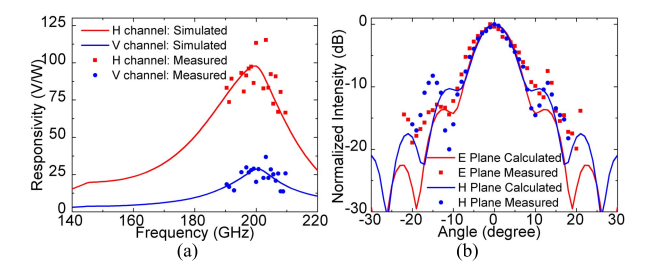


Fig. 4. (a) Simulated (solid lines) and measured (discrete points) responsivities versus frequency of each channel of the detector. (b) Calculated (solid lines) and measured (discrete points) radiation pattern in the E- and H-planes.

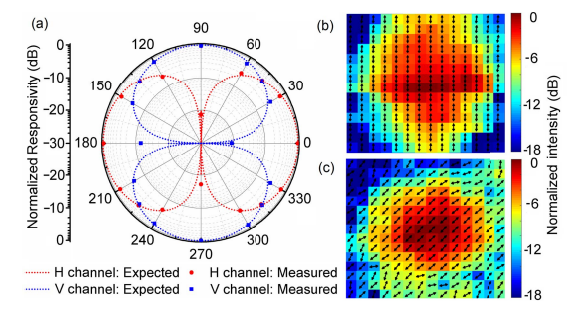


Fig. 5. (a) Normalized responsivities of two channels (discrete points) and their expected values (dotted lines) versus polarization angle  $\psi$ . Polarization imaging results of a (b) 90°-rotated and (c) 45°-rotated WR-5.1 horn antenna.

the output power. The simulated responsivities are plotted in Fig. 4(a) for comparison. The peak responsivity ( $R_{\rm peak}$ ) was obtained to be around 115 and 35 V/W at 203 GHz, for H and V channels, respectively. The ripples are likely from the standing wave effect [9]. The minimum NEP was estimated to be 15 pW/Hz<sup>1/2</sup>, as the output noise approaches the Johnson noise limit according to [13]. The isolation between the two channels was measured to be as high as 21 dB, consistent with the results in [16]. The optical loss from misalignment, mirror scattering, Gaussian coupling, and lens reflection is estimated to be  $\sim$ 10 dB and is excluded in these intrinsic responsivities [15].

The radiation patterns of the lens-coupled ASA in the E- and H-planes were obtained at 203 GHz. In this measurement, the THz multiplier chain was placed 25 cm from the detector, with its polarization aligned with the peak responsivity of the *H* channel of the detector. The detector was then mechanically scanned to measure the E- and H-plane radiation patterns. Fig. 4(b) compares the measured and calculation results obtained by using ray-tracing [16]; 3-dB beam widths of 10° and 9° were obtained in the E- and H-planes, respectively. The measurement results show a nearly Gaussian-shaped main beam in both planes and agree reasonably with the theoretical calculations. The discrepancy is primarily from the radiation of the second-order reflected wave between the lens surface and circuit ground [17].

## C. Polarization Measurement

The experimental setup for polarimetric detection at 203 GHz is the same as in Fig. 3. In this demonstration, the detector was rotated along the polar axis and the outputs of the two detector channels were measured, from which the responsivity for each channel can be obtained. These results were further corroborated by the polar plot of Fig. 5(a), which shows the normalized responsivities and the expected values as a function of the rotation angle  $\psi$  in Fig. 1(a) (which is

also the polarization angle). The expected values  $(R_{\rm exp})$  for the H and V channels after normalization were calculated from  $R_{\rm exp,H}=\cos^2(\psi)$  and  $R_{\rm exp,V}=\sin^2(\psi)$ , respectively. It can be seen that the normalized responsivities of the H channel closely follow a cosine-squared (sine-squared for the V channel) pattern. The small scatter is mainly from misalignment between the source and the detector. The results show that the two orthogonal components of the incoming linear polarized THz wave can be resolved and detected separately by the corresponding HBDs.

In addition to the polarimetric detection measurements, the polarization imaging capability of the detector has been demonstrated by using it as an imaging system. In this experiment, the transmitting field of a rotated WR-5.1 horn antenna at 8 cm was scanned by the proposed detector. The scanning step size was set to be 2 mm, and the imaging area is 2.8 cm  $\times$  2.8 cm (or 14  $\times$  14 pixels). For each pixel, the intensity I is taken as  $I = R_{\text{Norm},V} + R_{\text{Norm},H}$ , whereas the polarization angle  $\psi$  is calculated as  $\psi$  =  $\tan^{-1}((R_{\text{Norm},V}/R_{\text{Norm},H})^{1/2})$ . The imaging result containing the measured polarization direction is presented in Fig. 5(b) for 90°-rotated horn antenna and Fig. 5(c) for 45°-rotated horn antenna, respectively. The results show a nearly Gaussian beam, with measured beam diameter of  $\sim$ 2.6 mm which agrees well with the calculation result (2.46 mm). More importantly, the measured polarization directions at most pixels agree well with expectation, i.e., the same as rotation angle, with slight discrepancies at some pixels that are far away from the beam center due to the limited signal-to-noise ratio. The imaging results further demonstrate that the proposed detector can simultaneously detect both intensity and polarization.

### D. Discussion

The measured responsivities are relatively lower than the results in [15] using a similar diode stack, as well as that from Schottky diodes [18], [19] and SiGe HBTs [8], [9]. This reduced responsivity is consistent with the low measured  $\gamma$  for the devices in the integrated detector. We speculate that this may be due to the current leakage introduced by the gold atoms that diffused into the junction region during BCB curing. Based on prior experimental demonstrations of discrete HBDs, we expect that the responsivity can be improved to as high as  $\sim 3000$  V/W by employing HBDs with higher  $\gamma$ , as demonstrated in [15]. To the best of our knowledge, it is still the first time that two zero-bias HBDs were monolithically integrated into one compact and planar ASA for polarimetric detection. The detector demonstrated here can not only measure the intensity but also detect the polarization of the incident THz wave, therefore enabling a new class of THz detectors and detection technologies for many promising applications.

# V. CONCLUSION

In this article, a polarization-resolved planar detector based on two orthogonally integrated HBDs was presented for the first time to operate at room temperature in the mmW-THz region. The proposed detector can simultaneously measure the intensity and polarization of the incident EM wave, with improvable performance. The results indicate that the reported approach is promising for applications in advanced sensors and FPAs for remote sensing, biomedical imaging, and radio astronomy.

#### REFERENCES

- [1] D. M. Mittleman, M. Gupta, R. Neelamani, R. G. Baraniuk, J. V. Rudd, and M. Koch, "Recent advances in terahertz imaging," *Appl. Phys. B, Lasers Opt.*, vol. 68, no. 6, pp. 1085–1094, Jan. 1999.
- [2] K. Kawase, Y. Ogawa, Y. Watanabe, and H. Inoue, "Non-destructive terahertz imaging of illicit drugs using spectral fingerprints," *Opt. Exp.*, vol. 11, no. 20, pp. 2549–2554, Oct. 2003.
- [3] N. Gopalsami and A. C. Raptis, "Millimeter-wave radar sensing of airborne chemicals," *IEEE Trans. Microw. Theory Techn.*, vol. 49, no. 4, pp. 646–653, Apr. 2001.
- [4] D. L. Wu et al., "IceCube: Spaceflight demonstration of 883-GHz cloud radiometer for future science," Proc. SPIE, vol. 11131, Aug. 2019, Art. no. 1113103.
- [5] J. Bullock et al., "Polarization-resolved black phosphorus/molybdenum disulfide mid-wave infrared photodiodes with high detectivity at room temperature," Nature Photon., vol. 12, pp. 601–607, Aug. 2018.
- [6] K. Liu, M. Wang, C. Li, T. Chen, and S. Shi, "Development of a dual polarization SIS mixer with a planar orthomode transducer at 350 GHz," *IEEE Trans. Appl. Supercond.*, vol. 23, no. 3, Jun. 2013, Art. no. 1400705.
- [7] B. Dober et al., "Optical demonstration of THz, dual-polarization sensitive microwave kinetic inductance detectors," J. Low Temp. Phys., vol. 184, nos. 1–2, pp. 173–179, Jul. 2016.
- [8] J. Grzyb, M. Andree, R. Jain, B. Heinemann, and U. R. Pfeiffer, "A lens-coupled on-chip antenna for dual-polarization SiGe HBT THz direct detector," *IEEE Antennas Wireless Propag. Lett.*, vol. 18, no. 11, pp. 2404–2408, Nov. 2019.
- [9] Z. Li, B. Qi, X. Zhang, S. Zeinolabedinzadeh, L. Sang, and J. D. Cressler, "A 0.32-THz SiGe imaging array with polarization diversity," *IEEE Trans. THz Sci. Technol.*, vol. 8, no. 2, pp. 215–223, Mar. 2018.
- [10] S. Watanabe, "Terahertz polarization imaging and its applications," Photonics, vol. 5, no. 4, p. 58, Dec. 2018.

- [11] X. Wang, Y. Cui, W. Sun, J. Ye, and Y. Zhang, "Terahertz polarization real-time imaging based on balanced electro-optic detection," J. Opt. Soc. Amer. A, Opt. Image Sci., vol. 27, no. 11, pp. 2387–2393, 2010.
- [12] S. M. Rahman, Z. Jiang, P. Fay, and L. Liu, "Integration and fabrication of high-performance Sb-based heterostructure backward diodes with submicron-scale airbridges for terahertz detection," J. Vac. Sci. Technol. B, Microelectron., vol. 34, no. 4, Jul. 2016, Art. no. 041220.
- [13] Z. Zhang, R. Rajavel, P. Deelman, and P. Fay, "Sub-micron area heterojunction backward diode millimeter-wave detectors with 0.18 pW/Hz<sup>1/2</sup> noise equivalent power," *IEEE Microw. Wireless Compon. Lett.*, vol. 21, no. 5, pp. 267–269, May 2011.
- [14] D. J. Burdette et al., "Development of an 80 x 64 pixel, broadband, real-time THz imager," Proc. SPIE, vol. 8023, May 2011, Art. no. 80230F.
- [15] S. M. Rahman, Z. Jiang, M. I. B. Shams, P. Fay, and L. Liu, "A G-band monolithically integrated quasi-optical zero-bias detector based on heterostructure backward diodes using submicrometer airbridges," *IEEE Trans. Microw. Theory Techn.*, vol. 66, no. 4, pp. 2010–2017, Apr. 2018.
- [16] S. Raman and G. M. Rebeiz, "Single- and dual-polarized millimeterwave slot-ring antennas," *IEEE Trans. Antennas Propag.*, vol. 44, no. 11, pp. 1438–1444, Nov. 1996.
- [17] B. Ozbey and K. Sertel, "Distinct Gaussian properties of multiple reflections in extended hemispherical lenses," *J. Infr., Millim., THz Waves*, vol. 40, nos. 11–12, pp. 1053–1073, Dec. 2019.
- [18] L. Lei, J. L. Hesler, H. Xu, A. W. Lichtenberger, and R. M. Weikle, "A broadband quasi-optical terahertz detector utilizing a zero bias Schottky diode," *IEEE Microw. Wireless Compon. Lett.*, vol. 20, no. 9, pp. 504–506, Sep. 2010.
- [19] L. Liu, H. Xu, Y. Duan, A. W. Lichtenberger, J. L. Hesler, and R. M. Weikle, "A 200 GHz Schottky diode quasi-optical detector based on folded dipole antenna," in *Proc. 20th Int. Symp. Space THz Technol.*, Charlottesville, VA, USA, Apr. 2009, pp. 1–5.